URSI RCRS 2022, IIT (Indore), India, 1 - 4 December, 2022

Assessment of Surface Energy Fluxes variation with Land Cover Parameters using LandSat Satellite data

Ruchi Bala*(1), Vijay Pratap Yadav(2), D. Nagesh Kumar(1), Rajendra Prasad(3)
ruchibala7@gmail.com ; victory327759@gmail.com; dasikanagesh@gmail.com; rprasad.app@itbhu.ac.in
(1) Department of Civil Engineering, Indian Institute of Science, Bengaluru, India
(2) Department of Physics, Government PG, College, Obra, India
(3) Department of Physics, Indian Institute of Technology (BHU), Varanasi, India

Abstract

The urban heat island (UHI) is formed due to higher local temperatures in urban areas than surrounding rural areas. Impervious surfaces and vegetation are the two major land covers that have the capability to modify energy fluxes. The Latent Heat flux, Sensible Heat Flux and the Ground Heat flux was obtained for Bangalore city and ratio of fluxes to net radiation was calculated. The mean of ratio of each flux to net radiation was calculated for each land cover and found that the urban and bare soil region shows higher values of G/R_n as compared to the vegetated land covers. The urban land cover showed higher values of H/R_n as compared to the natural land covers and the vegetation and waterbody showed higher values of LE/R_n than other land covers. The relation of sensible heat flux with imperviousness and latent heat flux with vegetation was determined. The plot of H/R_n with ISF and LE/R_n with NDVI, both showed good positive relation.

1. Introduction

The urban heat island (UHI) is formed due to higher local temperatures in urban areas than surrounding rural areas. The increased human activity in the city has made this phenomenon more prominent. The urban thermal behaviour varies with land covers. Impervious surfaces and vegetation are the two major land covers that have the capability to modify energy fluxes. The study of surface energy fluxes with land cover parameters can be useful to understand its impact on UHI effect. The use of remote sensing data has increased in the study of land cover with different land cover parameters due to its synoptic and broad view over an area instantaneously. [1, 2]

Very few studies have been conducted on comparing sensible heat flux or latent heat flux with different land covers. Therefore, the spatial variation of heat fluxes with land covers and quantitative behaviour of land cover parameters with these fluxes needs to be explored.

2. Study area

Bangalore is the capital and lies in the southeast of Karnataka state in South India. It is considered as the largest city in South India and 27th largest in the world. Location map of study area is shown in figure 1 where the image of Bangalore city is represented as the false color composite image obtained from Landsat data.

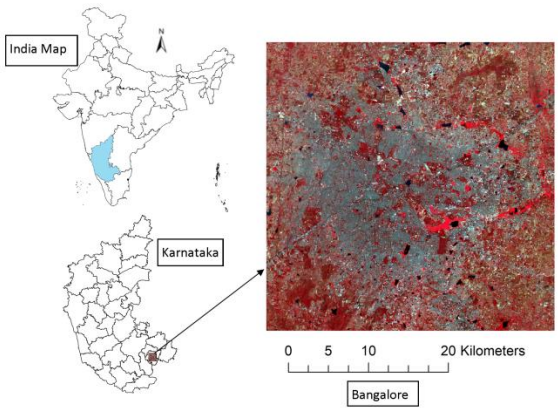

Figure 1. Location map of the study area.

3. Data and Methods

3.1 Data

The study was conducted for the date 11/01/2020 during day time (10:40 am). MCD18A2 provides

Moderate Resolution Imaging Spectro-radiometer (MODIS) Terra and Aqua combined data of Photosynthetic active radiation (PAR) at a spatial resolution of 1 km which was resampled to 30 m for study. Landsat-8 data was also used in the study for determining some land surface parameters. Further, India Meteorological Department (IMD) and IMDAA (from National Centre for Medium Range Weather Forecasting) data provides meteorological data for study. Specifications of the data used in the present study are shown in Table 1.

Table 1. Data specification

Data	Source
Surface albedo	LandSat
Shortwave Radiation	IMDAA
Surface emissivity	LandSat
Air Temperature	IMD
Surface Temperature	LandSat
Relative Humidity	IMDAA
Air Pressure	IMD
Photosynthetic Active Radiation	MODIS
Wind Speed	IMD

3.2 Methods

3.2.1 Determination of Surface Energy flux

$$R_n + A = G + LE + H \quad (1)$$

Here, R_n is the net radiation from natural land surfaces and can be calculated as

$$R_n = (1-\alpha)R_s + \varepsilon\varepsilon_a R_{L\downarrow} + \varepsilon R_{L\uparrow} \quad (2)$$

where, α is the surface albedo, R_s is the short-wave radiation, ε is the surface emissivity, ε_a is the atmospheric emissivity, $R_{L\downarrow}$ and $R_{L\uparrow}$ are the downward and upward blackbody radiations.

$$\varepsilon_a = 1.24\left(\frac{e_a}{T_a}\right)^{\frac{1}{7}} \quad (3)$$

$$e_a = RH \times e_s^* \quad (4)$$

$$e_s^* = 1013.25\, exp(13.318t_R - 1.9760t_R^2 - 0.6445t_R^3 - 0.1299t_R^4) \quad (5)$$

$$t_R = 1.0 - \frac{373.15}{T} \quad (6)$$

$$R_L\downarrow = \sigma T_a^4 \quad (7)$$

$$R_L\uparrow = \sigma T_s^4 \quad (8)$$

Where, e_a is the atmospheric water vapor pressure in hPa, T_a is atmospheric temperature in K, RH = relative humidity, e_s^* is the saturation vapor pressure in hPa, σ is Stefan's Boltzmann constant and T_s = surface temperature in K.

Sensible Heat Flux (H) is calculated as

$$H = \rho C_p \frac{T_s - T_a}{r_a} \quad (9)$$

where ρ = air density in kg/m^3, C_p = Specific heat of air at constant pressure, r_a = aerodynamic resistance in s/m.

$$r_a = \frac{ln\left(\frac{Z_m - d}{Z_{0m}}\right) \times ln\left(\frac{Z_h - d}{Z_{0h}}\right)}{k^2 u} \quad (10)$$

Z_m = height of the wind measurements, Z_h = height of the humidity measurements, d = zero plane displacement height, Z_{0m} , Z_{0h} = roughness lengths for momentum and heat transfer, k = von Karman's constant and u = wind speed in m/s^{-1}. The specific values of Z_{0m} , Z_{0h} and d was obtained from existing literature for different land covers. [3,4].

Latent Heat Flux (LE) was calculated as

$$LE = \frac{\rho C_p (e_s^* - e_a)}{\gamma(r_a + r_s)} \quad (11)$$

$$\frac{1}{r_s} = \frac{f_1(T_a) f_2(PAR)}{r_{sMIN}} + \frac{1}{r_{cuticle}} \quad (12)$$

Where, γ is the psychrometric constant and r_s is stomatal resistance, r_{sMIN} is the minimum stomatal resistance in s/m and was obtained for each land cover type from existing literature[5]. $r_{cuticle}$, $f_1(T_a)$ *and* $f_2(PAR)$ can be obtained as shown in Nishida et al 2003 [6]. $r_{cuticle}$ is the canopy resistance in s/m and can be a constant value.

Ground Heat Flux (G) can be calculated as

$$G = R_n - H - LE \quad (13)$$

3.2.2 Determination of Impervious Surface Fraction (ISF)

Linear spectral mixture analysis (LSMA) approach was used for calculation of fractions of the four endmembers contained in a pixel [7]. This is an image processing approach used for sub-pixel classification of land cover. The endmembers are determined by visual interpretation from the pure land covers from Landsat data. The linear mixture model is represented as

$$\overline{R}_b = \sum_{i=1}^{n'} \bar{f}_i \bar{R}_{i,b} + e_b \qquad (14)$$

where $\sum_{i=1}^{n'} \bar{f}_i = 1$ and $\bar{f}_i \geq 0$; $\bar{f}_i$ is the fraction of endmember i, $\overline{R_b}$ is the reflectance for band b, $\bar{R}_{i,b}$ is the normalized reflectance of endmember i in band b, n' is the number of endmembers and e_b is the residual. The fraction is determined using a least squares method by minimizing the residual e_b.

3.2.3 Calculation of Normalized Difference Vegetation Index (NDVI)

NDVI was obtained from Landsat-8 data using the equation (15). NDVI ranges from -1 to +1. The negative value of NDVI resembles waterbody whereas positive value with increase in magnitude resembles greater amount of vegetation.

$$NDVI = \frac{Band\ 5 - Band\ 4}{Band5 + Band\ 4}$$

4. Results and Discussions

4.1 Land Cover Classification

The Land Cover classification image was determined using maximum likelihood classification method from Landsat image and is shown in figure 2. This image reveals that the land cover surrounding the urban part mainly consists of bare land or less vegetated land cover (lawn or crop field). Some pixels of forests and waterbodies are also observed within the city.

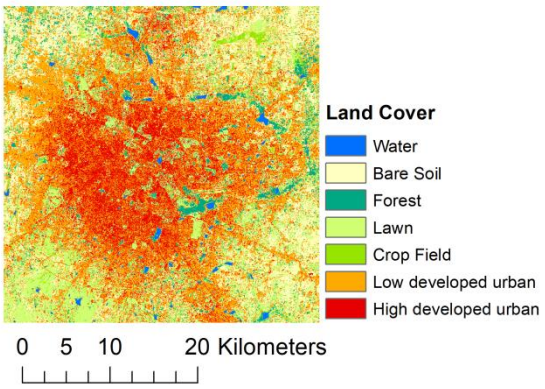

Figure 2. Land Cover image of the study area for date 11/02/2020.

4.2 Spatial Pattern of Surface Energy Fluxes

Figure 3 shows the spatial distribution of surface energy fluxes in the study area. The image reveals that G/R_n value for urban land covers show lower values whereas H/R_n shows higher values as compared to the major natural land covers around the city. LE/R_n shows greater values for dense vegetated land cover. For detailed analysis of fluxes value, mean of ratio of each flux to net radiation was calculated for each land cover and shown in Table 2.

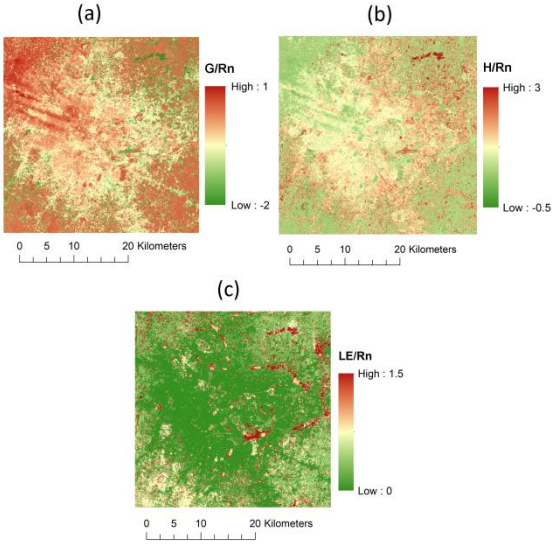

Figure 3. Ratio of Surface Energy fluxes to net radiation (a) G/R_n, (b) H/R_n and (c) LE/R_n

Table 2. Mean ratio of Surface Energy fluxes to net radiation for each land cover

Land Cover	G/R_n	H/R_n	LE/R_n
Water	0.337	0.049	0.614
Bare Soil	0.564	0.229	0.207
Forest	-0.263	0.159	1.104
Lawn	0.436	0.166	0.398
Crop Field	-0.178	0.192	0.986
Low developed urban	0.664	0.336	0
High developed urban	0.502	0.498	0

Considering G/R_n, The urban and bare soil region shows higher values as compared to the vegetated land covers. During day time, ground heat flux is the energy transferred from the surface into the ground because the temperature below the surface is generally lower than the surface. This is analogous to the thermal inertia property of land covers. Considering H/R_n, the impervious land covers (urban) shows higher values as compared to the pervious land covers (water, bare soil and vegetated land covers). Sensible heat flux increases with surface temperature and transferred from the surface to the atmosphere [8]. Since, more of anthropogenic activity is observed in urban areas which increase the temperature; the urban land cover shows higher sensible flux values. Considering LE/R_n, forest, crop field and waterbody show higher values than other land covers. This is because latent heat is produced by

evapotranspiration of vegetation and evaporation of waterbodies.

4.3 The relation of heat fluxes with NDVI and ISF

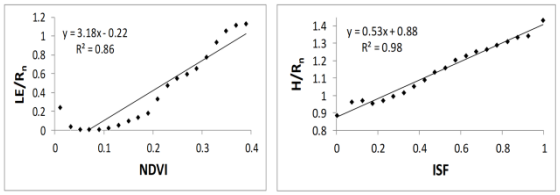

(a) (b)

Figure 4. The plot of (a) LE/R_n with NDVI (b) H/R_n with ISF

Figure 4 shows that the plot of H/R_n with ISF shows good positive relation which reveals that increase in impervious land cover results in increased sensible heat flux. Thus, urbanisation increases the sensible heat flux in the city. The plot of LE/R_n with NDVI shows positive relation for positive NDVI values. Water pixels were excluded for this analysis because it shows higher LE/R_n and negative NDVI values. Thus, LE/R_n show good positive relation (by excluding water pixels) which reveals that increase in vegetation results in increased evapotranspiration which raises the latent heat flux.

5. Conclusions

The Latent Heat flux, Sensible Heat Flux and the Ground Heat flux image was obtained in the study for Bangalore city and ratio of fluxes to net radiation was calculated. The spatial pattern of these fluxes were shown which reveals that G/R_n value for urban land covers show lower values whereas H/R_n shows higher values as compared to the major natural land covers around the city. LE/R_n shows greater values for dense vegetated land cover. Further, mean of ratio of each flux to net radiation was calculated for each land cover and found that the urban and bare soil region shows higher values of G/R_n as compared to the vegetated land covers. The impervious land covers (urban) showed higher values of H/R_n as compared to the pervious land covers and the forest, crop field and waterbody showed higher values of LE/R_n than other land covers.

The relation of sensible heat flux with imperviousness and latent heat flux with vegetation was determined. The plot of H/R_n with ISF and LE/R_n with NDVI, both showed good positive relation.

Acknowledgement

The author thankfully acknowledges the financial support provided by Department of Science and Technology (DST), New Delhi, India, under the scheme of Science and Engineering Research Board (SERB) National Post-Doctoral Fellowship (PDF/2021/000202).

References

1. J. A. Voogt & T. R. Oke, “Thermal remote sensing of urban areas,” Remote sensing of Environment, vol. 86, pp. 370-384, 2003.

2. Bala, R., Prasad, R., & Yadav, V. P. (2020). A comparative analysis of day and night land surface temperature in two semi-arid cities using satellite images sampled in different seasons. Advances in Space Research, 66(2), 412-425.

3. Grimmond, C. S. B., King, T. S., Roth, M., & Oke, T. R. (1998). Aerodynamic roughness of urban areas derived from wind observations. *Boundary-Layer Meteorology*, *89*(1), 1-24. 95, 2014.

4. Moriwaki, R., & Kanda, M. (2006). Scalar roughness parameters for a suburban area. *Journal of the Meteorological Society of Japan. Ser. II*, *84*(6), 1063-1071.

5. Kato, S., & Yamaguchi, Y. (2007). Estimation of storage heat flux in an urban area using ASTER data. *Remote Sensing of Environment*, *110*(1), 1-17.

6. Nishida, K., Nemani, R. R., Running, S. W., & Glassy, J. M. (2003). An operational remote sensing algorithm of land surface evaporation. *Journal of Geophysical Research: Atmospheres*, *108*(D9).

7. Wu, C., & Murray, A. T. (2003). Estimating impervious surface distribution by spectral mixture analysis. *Remote sensing of Environment*, *84*(4), 493-505.

8. Kato, S., & Yamaguchi, Y. (2005). Analysis of urban heat-island effect using ASTER and ETM+ Data: Separation of anthropogenic heat discharge and natural heat radiation from sensible heat flux. *Remote Sensing of Environment*, *99*(1-2), 44-54.